Design and Use of a Penetrating Deposition Nozzle for Z-Pinning Additive Manufacturing

Brenin Bales[1], Roo Walker[1,2], Deepak Pokkalla[1,2], Seokpum Kim[2], Vlastimil Kunc[2], Chad Duty[1,2]

[1]University of Tennessee
Knoxville, TN

[2]Manufacturing Science Division
Oak Ridge National Laboratory
Oak Ridge, TN

Abstract

Fused Filament Fabrication (FFF) involves depositing material layer-by-layer to create a three-dimensional object. This method often demonstrates high mechanical anisotropy in the printed structure, leading to a drop in the material strength of the part when comparing structures along the deposition plane (X/Y-Axis) versus across layers in the build direction (Z-Axis). Initial efforts to improve anisotropy led to the development of the Z-Pinning process, where continuous pins are deposited across layers in the Z-Axis. Z-pinning has demonstrated significant gains in toughness and inter-layer strength, particularly in fiber-reinforced materials. However, this process can also create flaws in the structure that increase in severity and frequency as the pins grow in length and diameter. To mitigate this, a penetrating nozzle has been developed that extends a fine-tipped extrusion nozzle deep into the pin cavity and simultaneously extrudes material as it retracts. This study investigates the printability of the penetrating nozzle for simple geometries and evaluates the resulting Z-pinning mesostructure. As a result of this study, the prototype penetrating nozzle design was analyzed and built. Through a pressure driven flow analysis it was determined that filament will flow through the penetrating nozzle as the system pressure drop of 9.3 Mpa is less then the minimum critical pressure of 12.07 Mpa. Additionally, it was after a transient thermal simulation, it was found that after a pause of 15 seconds the system can resume printing with no drop in heat at nozzle exit. This means the additional length of the penetrating nozzle, will not cause any clogs during any pauses in filament flow.

Introduction

Additive manufacturing (AM) is one of the fastest growing technologies for both metals and polymers in the manufacturing industry. Primarily due its lack of tooling required, design freedom, and lower cost per part created [1]. One of the most popular methods of additive manufacturing is the material extrusion process known as fused filament fabrication, first pioneered by Scott and Lisa Crump as fused deposition modeling (FDM) with Stratasys [2]. The FFF/FDM method involves extruding thermoplastic (in a filament feedstock) through a nozzle to create a printed structure build along the X and Y axis on a build platform. The material extrusion occurs in a layer-by-layer fashion on the build plate, building up in the Z-axis. Due to the layer-by-layer build pattern, FFF printed structures are highly anisotropic, leading to drops in strength. This drop in strength is most severe when the load direction is orthogonal (90º) to the print direction (Z-axis) The best and strongest material properties are seen then the printed structures are tested so that their material beads are aligned (0º) in the load direction[3–5]. Due to the high anisotropy seen when comparing samples in the Z-axis (across build layers) to X-Y plane, forces are transmitted through the adjoining layers in the Z-axis along discrete interfaces between material beads on the X-Y plane [6]. Depending on the printing system and material the reduction in strength can range from 25% to 97% [7–13]. Specifically, across both large (BAAM and LSAM) and small scale systems PLA shows a drop in strength ranging from 33% to 57% across the X and Z-axis [7,8]. Neat ABS and Fiber Reinforced ABS across BAAM and LSAM large scale systems and small scale FFF systems shows a greater range of strength reduction. Ranging from 25% to 97% reduction in ultimate tensile strength [7,9–13].

Researchers at a variety of institutions have developed methods to combat the high anisotropy found in FFF printed structures. Primarily the methods attempt to increase the inter-layer bond strength by increasing inter-diffusion of molecular chains across layers. Increasing the inter-diffusion of polymer chains across the interface can be controlled by keeping the print temperature of the material above the glass transition temperature of the material [14–16]. An example can be seen in a collaboration between the University of New Mexico and Texas-Austin. The method developed by the two university research teams demonstrated a 50% increase in ultimate tensile strength across print layers (Z-axis) by increasing the extrusion multiplier values over their stock settings. Additionally, this method saw a 10% increase in X-axis ultimate tensile strength and the ability to print near isotropic structures [17]. Other research has been focused on adding a pre-heating method just before deposition of new material. Oak Ridge National Laboratory (ORNL) developed a process for the BAAM (Big Area Additive Manufacturing) system in which infrared laps are mounted to the printing head. This system led to a doubling of the fracture energy in 20% CF-ABS printed structures [18]. A research group from Arizona State University developed a method to increase the temperature of the build surface by using a laser aimed at the surface preceding where the filament will fall. This method increased the flexural strength of 0.03% Carbon Black ABS by 95% [19]. A team from the University of Tennessee and ORNL sough to alleviate the high anisotropy and drop in strength through the creation of the novel Z-pinning method, which was introduced at the 2017 SFF conference [20].

Z-Pinning

The Z-pinning for AM process can be largely broken down into four steps that define how the structure is printed. The AM Z-pinning process will start with the deposition of the surrounding structure (the structure that is being pinned). For testing purposes this surrounding structure is a rectilinear grid, as seen in **Figure 1a**. During this stage, a predetermined number of layers are printed (set by the pin length) and the pin cavities are created by leaving gaps in the structure itself. **Figure 1b** demonstrates the pinning process, here the nozzle will be positioned directly over the pin cavity and deposit material to fill a prescribed amount of the pin cavity. This process is then repeated in **Figure 1c and 1d** during these stages more of the surrounding structure is printed, and another pin is deposited at the alternative position. This process repeats for the entire structure (**Figure 1e and 1f**). It should be noted that the pins are staggered so the seams of the pins are not all on one layer.

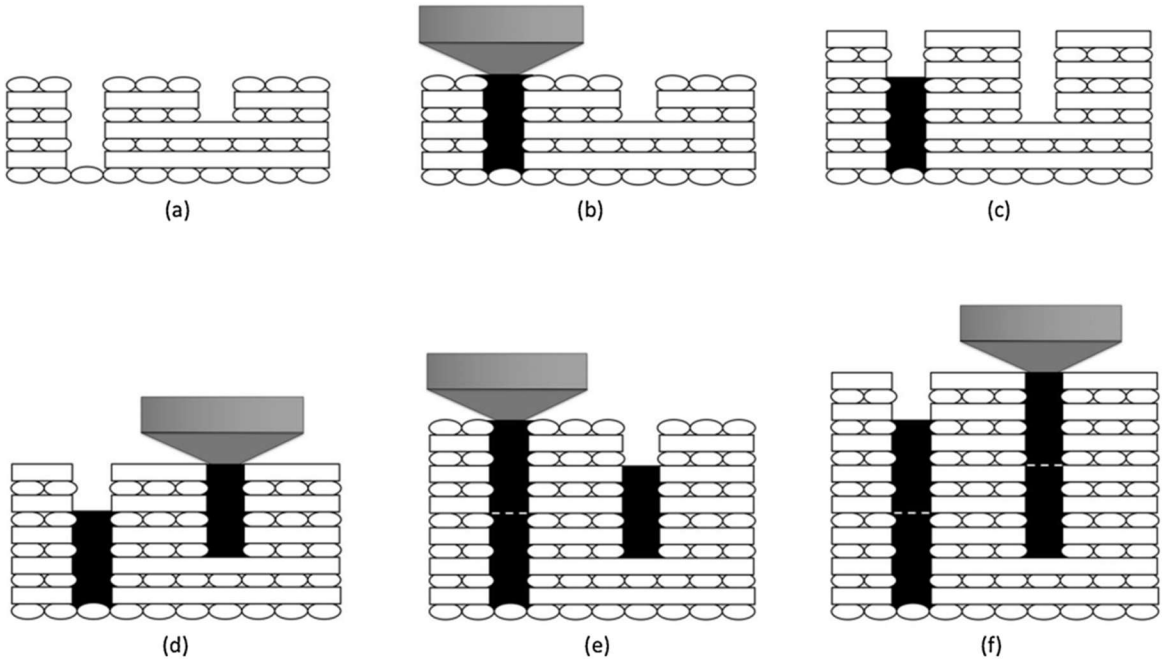

Figure 1: The AM Z-Pinning Process [21]

Z-Pinning Parameters

The pin dimensions that determine how much existing structure is deposited or how much material is extruded into the pin cavity make up the Z-pinning parameters used in the Z-pinning process. The Z-pinning parameters are defined as the width and length of the pin, as well as the infill percentage and seam offset (**See Figure 2**). The pin widths used in AM Z-pinning are defined as an integer multiple of the exit diameter of the nozzle, which is defined as "W" (W=0.5mm). For the initial Z-pinning studies the typical tested diameters were 1.5mm, 2mm, and 3mm. These are defined in studies as 3W, 4W, and 6W respectively. The second pin parameter that is defined is the pin length. This is simply the number of layers that the pin will occupy (**Figure 1b and 1d** for example). Initial investigations were focused on three pin lengths: an 8-layer, 12-layer, and 20-layer pin. These are defined in combination with the seam offset that is applied so that all the pin interfaces do not form one line across the structure (**See the circles in Figure 2**). The seam offset for all studies is held at half the length of the pin (L). This means

that pins are deposited in the other pin position after L/2 layers of structure have been printed. The final pin parameter is the infill percentage of the pins themselves. This is the amount of material that is extruded in the pin cavity. It is defined as the amount of material deposited compared to the theoretical volume of the cavity in which it is being deposited. For the AM Z-pinning process three infill percentages were investigated, 80%, 100%, and 120%. Overfill at 120% was possible due to the sparse nature of the rectilinear grid that is printed as the surrounding structure (**See Fig. 2**).

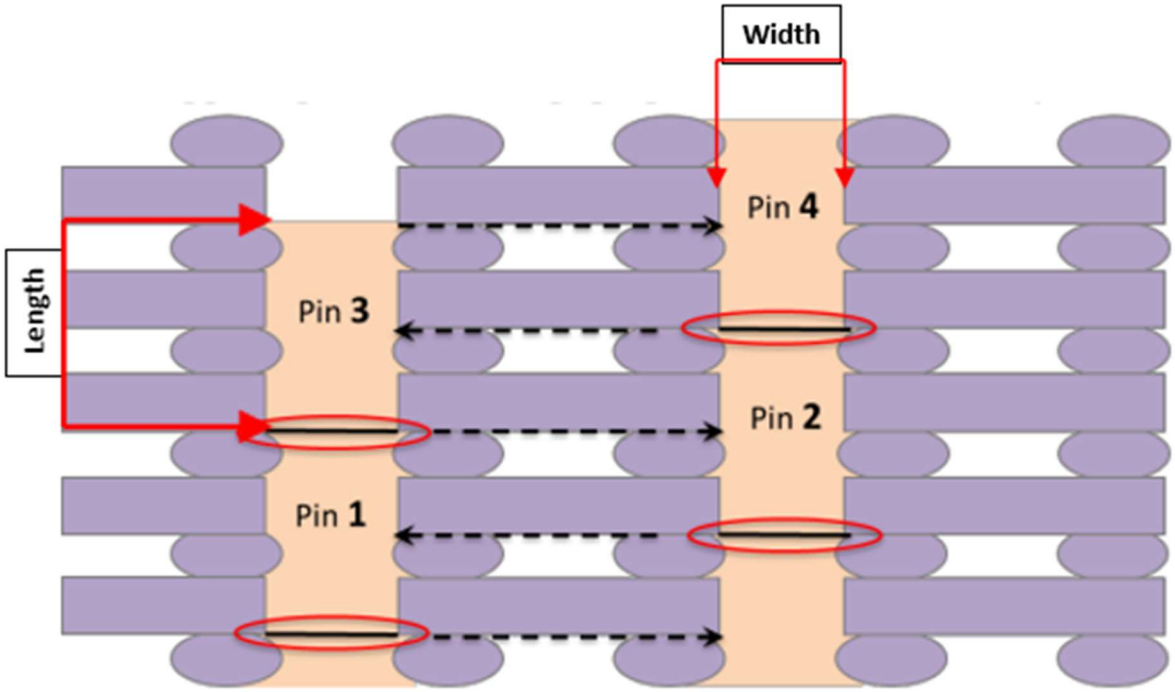

Figure 2: AM Z-pinning parameters [22]

Initial Studies in Z-Pinning

Initial work in Z-pinning for additive manufacturing focused on reducing anisotropy found in FFF printed structures by improving the Z-axis ultimate tensile strength, leading to the development of quasi-isotropic properties [21]. Of the pin parameters studied, the pin length, width, and seam offset were kept constant with only pin infill increasing from 0%-120%. Additionally, a solid sample was also produced to determine maximum strength of the sample [21]. This study was able to demonstrate that as the pin infill increased from 0% to 120%, toughness, stiffness, and ultimate tensile strength all increased. The data also showed that as the Z-axis ultimate strength increased with pin infill, the degree of anisotropy present in the structure would decrease as well [21].

Subsequently, another round of research was conducted that expanded upon the initial pin parameter set. This work investigated larger pin diameter of 2 mm and 3 mm, while also increasing the pin lengths tested from 8 layers to 12 and 20 layer pins [23]. This initial study further reinforced initial findings: as pin infill increased, so did the mechanical properties in both X- and Z- directions. Additionally, it was discovered that increasing the pin diameter and length

increased tensile properties as well as lowered the degree of anisotropy present in the samples [23]. This can be seen most prevalent in the 80% sample set shown in **Figure 3**. Shown above in **Figure 3**, this 80% pin infill samples with a pin diameter of 1.5mm (3W) showed an increase of strength across Z-axis when moving from an 8 layer pin to a 20 layer pin. This again could be seen in the 2mm diameter pins (4W) in the X-axis ultimate tensile strength [23]. Yet, one of the chief results of this study was the discovery and further reinforcement of the fact that defect propagation negatively impacted the effectiveness of longer and wider pins.

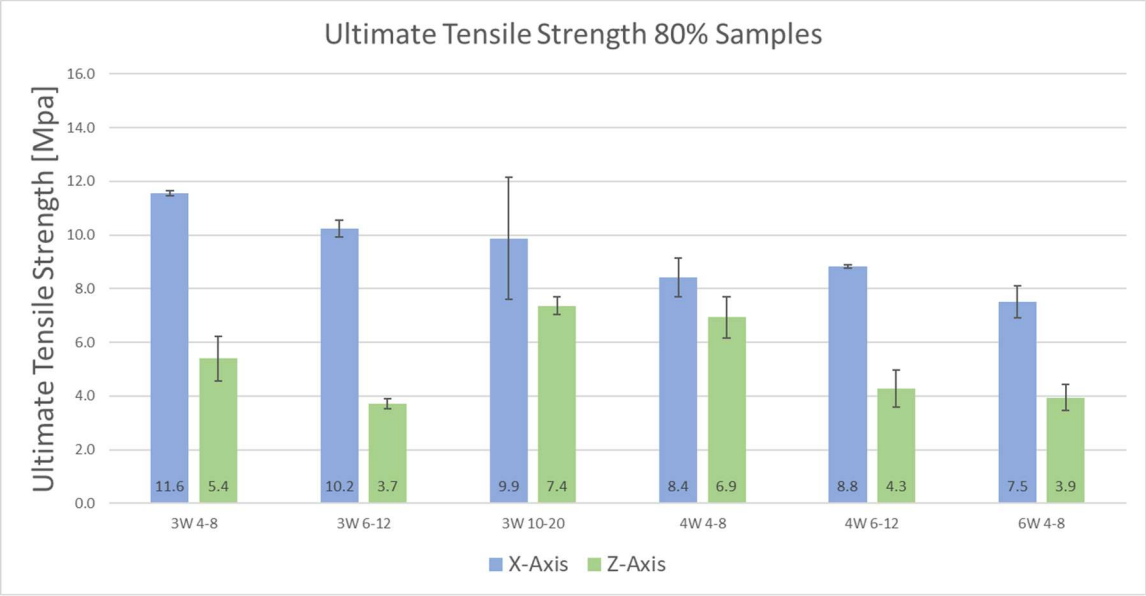

Figure 3: Ultimate Tensile Strength of 80% Infill Samples [23]

Defects

Results from the initial rounds of AM Z-pinning concluded that as pin infill, length, and width increased, as did the mechanical performance of the print. Yet, defects in the printing process saw a decrease in mechanical performance where greater performance was expected (See **Figure 4**). To understand the defects, it is important to separate the Z-pinning process into two phases. The first phase is the rectilinear grid, in which nearly no defects occur. The second phase is the pin deposition. The pin deposition is where the error propagation occurs in the AM Z-pinning process. For a successful pin deposition to occur, material must be dropped cleanly and completely into the pin cavity (See **Fig. 2**). Shown in **Figure 5** are the two flaws during the AM Z-pinning process. First is the underflow condition (See **Fig 5a**), otherwise known as "rope in a bucket" [24]. This process occurs when material does not flow cleanly into the pin cavity, this causes small voids that span the entirety of the pin cavity (see **Fig. 4**). The second defect (**Fig 5b**) is the over-fill condition, otherwise known as "short shot". This error occurs when the material does not fall completely into the pin cavity. This leads to a large defect at the bottom of the pin, while simultaneously leading to a large amount of material bonding on the print surface. In addition to the drops in material strength that occurs due to the voids that are

created in pin cavities, the short shot error will cause an excess of material to build up on the print surface. This will lead to a total print failure when two much material will harden and cause the nozzle to run into the nodule and knock the print over.

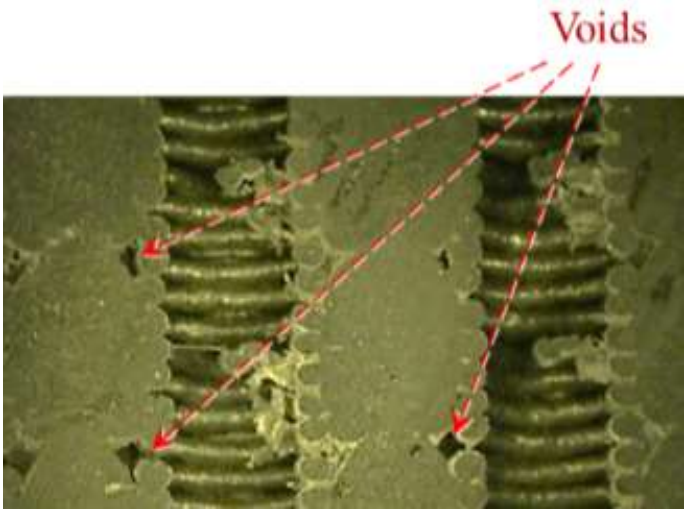

Figure 4: Voids in Z-pinning process [25]

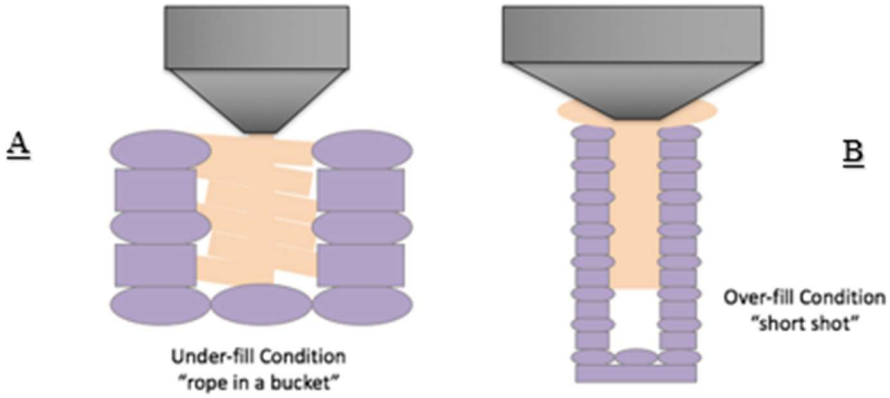

Figure 5: Flaws during the printing process: Creation of voids (A) and Overflow (B) [24]

Penetrating Nozzle Approach

As a result of the defects found in the AM Z-pinning process a modification to the FFF extruder hot end to alleviate the two failure modes. This solution was the novel penetrating nozzle [24]. The penetrating nozzle approach would involve developing an extended nozzle to penetrate the pin cavity and simultaneously deposit material while retracting (See **Figure 6**). The goal of this novel approach would be to create longer Z-pins that penetrate more completely into deeper pin cavities. Having a more complete fill of the pin cavity would in theory allow for a higher successful infill percentage as well as greater mechanical interlocking with the walls of the cavity [26].

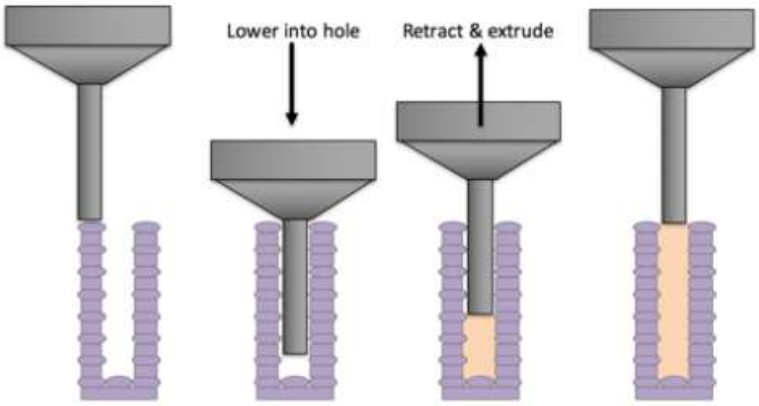

Figure 6: Penetrating Nozzle Approach [24]

When making such significant modifications to critical component of the extruder, it is important to understand the effects the extended nozzle design might have on the hotend. Two questions had to be answered during the design process to inform how the nozzle should be built and could function. First, can material flow through the nozzle? And second, can the nozzle and hotend stay hot during different stages of the printing process, especially during a pause in printing?

Design Process

To answer these questions, two experiments were conducted. First, a pressure drop analysis predicted whether liquid filament would be able to flow through the nozzle. This involved measuring the rheological properties of the polymer and evaluating a viscoelastic printability model at various extrusion conditions [27]. Then, a transient thermal analysis was conducted using a 3D model of the penetrating nozzle design. These results were steady state thermal analysis and by extruding material through a penetrating nozzle.

Before the pressure drop analysis or thermal analysis could be conducted, a prototype of the nozzle was designed. The printer platform selected for this project was a Prusa Original MK3s+. This printer allows for a high degree of repeatability while still allowing easy customization. The penetrating nozzle design was composed of two discrete additions to the hotend. First, the nozzle selected was a 1/8 NPT 22 Gauge Stainless Steel Dispensing Needle with a nickel-plated brass base [28]. This nozzle was chosen not only for its similar exit diameter to stock FFF nozzles (0.4mm), but also the combination of materials. Nickel-plated brass in the threaded base would allow for improved thermal performance where the softer material would not be subjected to high stresses. The stainless-steel nozzle would benefit from higher material strength, which is critical considering how thin the walls of the nozzle are. The second addition to the nozzle was a 1/8 NPT to M6 threaded adaptor [29] to interface with the stock heater block and provide the beneficial thermal properties of Nickel-plated brass. Seen in **Figure 7**, the penetrating nozzle was then cut down to a final length of 5mm, allowing for 20 layers of full penetration. This allows the penetrating nozzle to penetrate up to the longest pins previously studied and allows longer pins to be studied.

Figure 7 Penetrating Nozzle Prototype

Pressure Driven Flow Analysis

The pressure driven flow analysis was based on a printability model that incorporates a variety of material extrusion parameters in order to create a model of how "well" a printer can extrude material [27]. This occurs by defining the three critical pressures that the system will experience and determining the minimum of the three critical pressure values. This will be the limiting force that can be applied during material extrusion in order for material to flow successfully. The three critical pressures used in this experiment are motor driving, motor drive with slip, and finally Euler's buckling pressure.

Critical Pressure Values

The first step in the pressure driven flow analysis is to determine the three critical pressure value that the system will experience. To do this a variety of parameters from the motor and extruder design need to be determined. The equations described below refer to the three pressures that the system will experience. Motor driving pressure without slip is the maximum torque of the motor (F_d) divided by radius of the driving wheel (A_f). If this force exceeds the sheer strength of the filament being extruded, a second force must be investigated. This is the motor driving pressure with slip, where the maximum shearing force must be calculated (F_f).

The last force that is investigated is the buckling pressure. If the buckling pressure is the minimum value, then the filament material will buckle under the force during the extrusion process [27,30]. The equations and values for these can be seen below in **Table 2.** As can be seen in **Table 2** the minimum critical pressure is motor driving with slip, meaning that as soon as the motor pushes over 12.07 MPa onto the filament, the drive gears will "slip" causing material to fail to flow. Once this minimum critical pressure was determined the next step was determining the maximum pressure drop that the custom penetrating nozzle system will experience.

Table 1: Critical Pressure Values [27,30]

Critical Pressures		
Motor Driving Pressure (no slip)	$\frac{F_d}{A_f}$	18.88 [Mpa]
Motor Driving Pressure (slip)	$\frac{F_f}{A_f}$	12.07 [Mpa]
Euler's Buckling Pressure	$\frac{\pi^2 E d_f}{16L^2}$	461.78 [Mpa]

Pressure Drop Analysis

To better understand the printability and rheological behavior of neat PLA within this novel nozzle design, the material was analyzed using parallel plate rheology on a Discovery Hybrid Rheometer (DHR). An oscillatory frequency sweep at 225 C from 0.1-628 rad/s was performed on a 25 mm plate with a 1.0 mm gap and a strain percentage of 0.5% [30]. It was found that the neat PLA was shear thinning above 100 rad/s, which determined the region of interest when analyzing the pressure drop. The pressure drop equation is defined below in [1]. To calculate this, the viscosity and shear rate through the nozzle must be determined.

$$\Delta P = \frac{8\eta Q L}{\pi R^4} \quad [1]$$

Most additive manufacturing polymers are shear thinning which implies that the shear rate influences the viscosity (η). This can be described with a power law relationship defined by:

$$\eta = C\dot{\gamma}^{n-1} \quad [2]$$

where *n* is the power law index and C is a constant called the co. The Rabinowitsch-corrected shear rate through a nozzle [32] is defined by:

$$\dot{\gamma} = \frac{4Q}{\pi R^3}\left(\frac{3n+1}{4\mathrm{n}}\right) \quad [3]$$

Utilizing the above power law related equations [2] and [3], the pressure drop [1] can be found. The pressure drop equation [1] and the power law viscosity equation [2] utilize steady-state viscosity (η), in order to relate the complex viscosity (η^*) values that were observed with parallel plate rheology to the viscosity experienced during FFF processing, the Cox-Merz rule was applied [Eqn. 4]. The Cox-Merz rule states that the shear-rate dependency of steady-state viscosity (η) is equivalent to the angular frequency (ω) dependency of the complex viscosity (η^*) [33].

$$\eta(\dot{\gamma}) = \eta^*(\omega)_{\dot{\gamma}=\omega} \quad [4]$$

The shear rate and viscosity values will change based on their location in the extruder, shown in **Figure 8**. These values are gained through inputting the data gained from rheological tests into the series of equations listed above (Equations [1-4]). The results of these are shown in **Table 3**. These values are then inputted all into the pressure drop equation [1]. This is the final step in the pressure drop analysis and yielded a value of 9.3 MPa. As a result of our system pressure drop being less than the critical pressure derived in **Table 2**, the neat PLA filament can flow through the system.

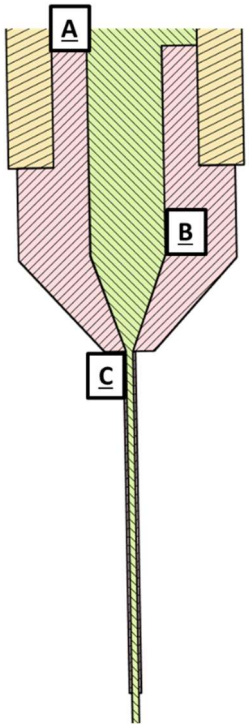

Figure 8: Section view of Penetrating Nozzle

Table 2: Rheological Parameters used in Calculations

Parameter	Entry (A)	Middle (B)	Exit (C)
C [PaS^n]	19,994		
Shear Rate [1/s]	0.87	25.9	808.4
Viscosity [PaS]	2082	730	252

Transient Thermal Analysis

The next step was modeling the polymer flow through the extruder during the Z-pinning process investigate how the process might affect filament heating/cooling and flow. In order to do this a model of the hotend was created on AutoDesk CFD 2021 with a volumetric flow rate that mimics the printing and pause steps that occur during the Z-pinning process. The print – pause – print transition steps are critical to understand because of the extra length of the nozzle will affect how thermal characteristics of the polymer (due to travelling farther from the heating element). In this step, the nozzle will have just finished fresh pin layer before moving back across the surface of the structure slowly back to the home position at the start of the printed structure before the deposition of another layer will occur. This step will roughly take 15s in which no filament is being extruded, but the heating element still holds the printing temperature. The purpose of this study is to investigate the thermal properties at the very tip of the nozzle, in order to ensure that the filament at the nozzle tip will not cool below 180ºC, which was determined to be the point in which filament flow is inconsistent and material will not extrude on the stock nozzle.

Model Creation and Setup

The model created for the simulations was the prototype hot end assembled on the Prusa FFF system (See **Figure 9**). The materials assignments in the 3D model set according to the prototype's construction and properties were defined by the standard values found in Autodesk material library. This was then experimentally verified by conducting a steady state analysis with no filament present meaning no material flow, just a static heat value and boundary conditions. This was verified by creating Arduino thermistor circuit and measuring various points around the base of the nozzle and adaptor, they were found to be within 2ºC of the steady state simulation [34]. Shown in **Table 4**, the materials chosen for the project were 304-Stainless steel for the penetrating nozzle and heartbreak, brass for the threaded adaptor and nozzle base, and standard aluminum for the heater block. Additionally, due to the rheological analysis performed for the pressure drop analysis, the filament was fully and accurately modeled.

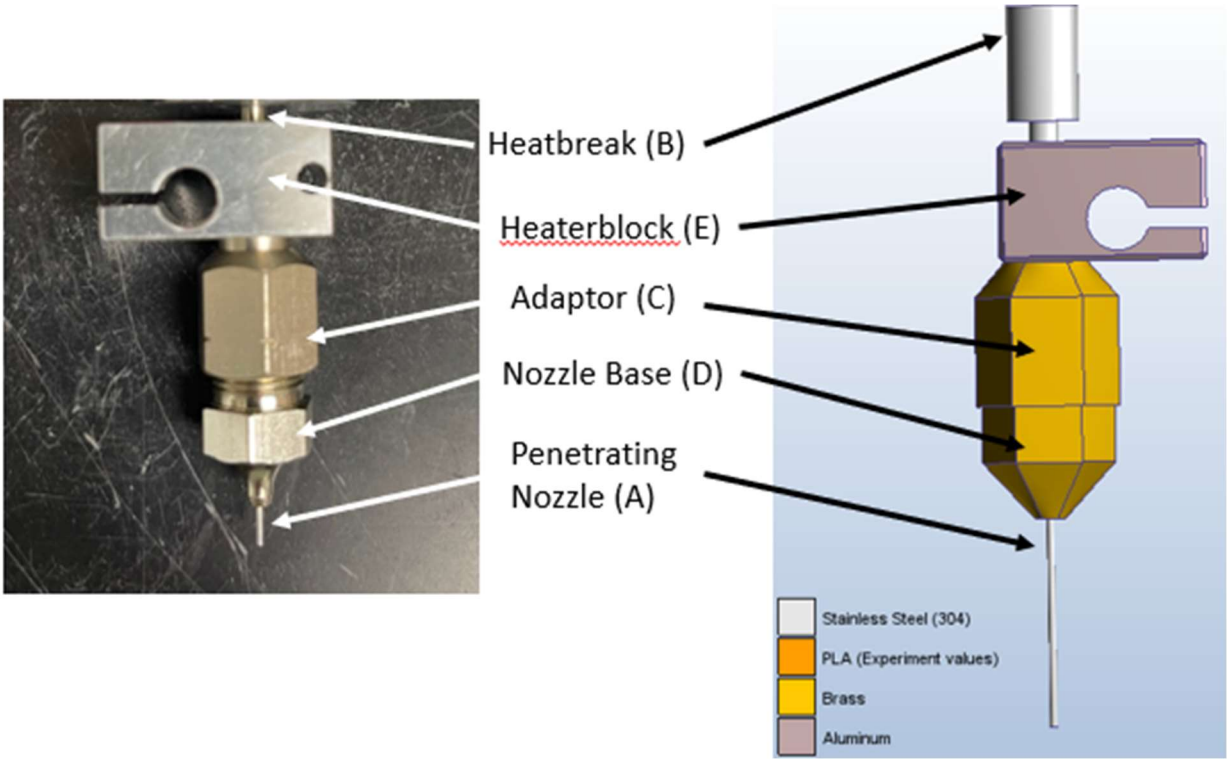

Figure 9: Prototype and CFD Model and Material Locations

Table 3: Material Assignments for Prototype Nozzle

Material	Assignment
304-Stainless Steel	Nozzle (A) and Heatbreak (B)
Brass	Threaded Adaptor (C) and Nozzle Base (D)
Aluminum	Heaterblock (E)

Simulation Methodology

The model was constrained in order to accurately model the effect that not only the surrounding air and environment will have on the heat end, but what the filament will do as it is extruding during the printing process. As such, both radiation, film coefficient, and convection are modeled. Radiation emissivity values were applied to all surfaces (external and internal faces) according to the standard values of the material present in combination with the background temperature of the face. The film coefficient was applied to all faces in which contact with air was possible and set according to the standard values of the various materials, as well as the background temperature. As a feature of Autodesk CFD's solver, conduction was applied for all materials in the build. The only external surfaces that did not have a radiation or a film coefficient was the heaterblock (see Figure above). This was done to keep the temperature of the heaterblock itself at a consistent 225ºC (the printing temperature). To do this, a static

temperature value was applied to all external and internal faces of the heaterblock. In addition, the exit and entrance temperatures of the heatbreak were set mimic how the what temperature gradients the filament will experience as it is traveling into the liquefier zone inside the heaterblock [35]. This ensures that as it enters and exits the liquefier zone the filament will maintain the temperatures it does during the printing process. Convection was not applied to the hotend due to the hotend fan not running during Z-pinning, as a result there was no forced convection boundary conditions present. Lastly, a volumetric flow rate is set to allow the filament to pause while the extruder is heating, print for 270 seconds, pause for 15 seconds, then finally printing again for 120 seconds, a graph of the volumetric flow behaviors is shown below in **Figure 9**. The flow rate itself is set for the 4.792 mm^3/s, which is the lowest flow rate the material is deposited at during the process. A full model, with constraints can be seen below in **Figure 10**.

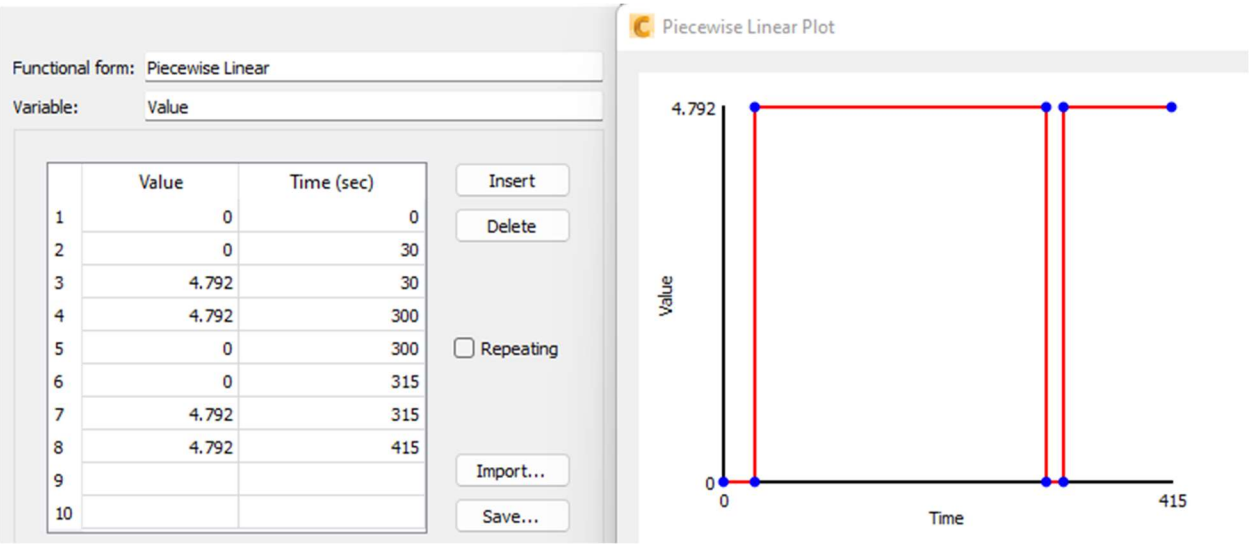

Figure 9: Volumetric Flow Rate Values, Units in mm^3/s

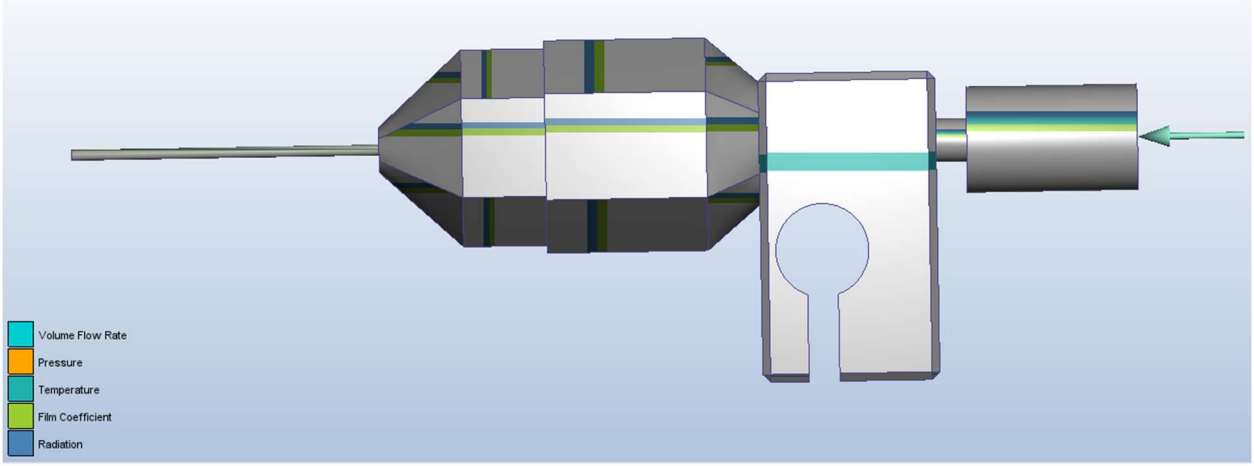

Figure 10: Full Penetrating Prototype, with constraints

The model was meshed by Autodesk CFD using the automatic meshing software tetrahedral elements. The maximum size for all edge elements created was 10 mm, with a minimum refinement length of 0.037 mm. While surface meshes had a maximum size of 0.002 mm. Then an automatic surface refinement was applied to all surfaces to reduce the element count to 86k elements (both solid and fluid). Once the model was meshed , the simulation was run as a transient solution with a step size of 0.08 seconds with 3 inner iterations per time step. This resulted in a full convergence of all values calculated by the solver.

Results

After running the simulation for the full time span the model converges. **Figures 11** and **12** are the thermal maps of the penetrating deposition nozzle and extruder. Shown in **Figure 11** is the extruder right at the end of the printing process, specifically one second away from the pause stage (See **Fig. 9**). Clearly shown on the left end on the heatbreak, the filament is still solid while at 35ºC, yet as it enters the heaterblock, it will rapidly heat up and become liquid at 225ºC. **Figure 12** critically, shows the thermal map of the extruder after the pause stage ends. It is important to note that due to fresh, cold filament not being pushed through the extruder, the stationary filament is able to entirely heat up to 225ºC. Due to the lack of extrusion this heat will then creep back up the heatbreak and into the heatsink (not shown). In a full experiment, a fan will be positioned perpendicular to the heatsink in order to keep the entire heat sink (and filament inside it) to roughly 30ºC - 40ºC [35].

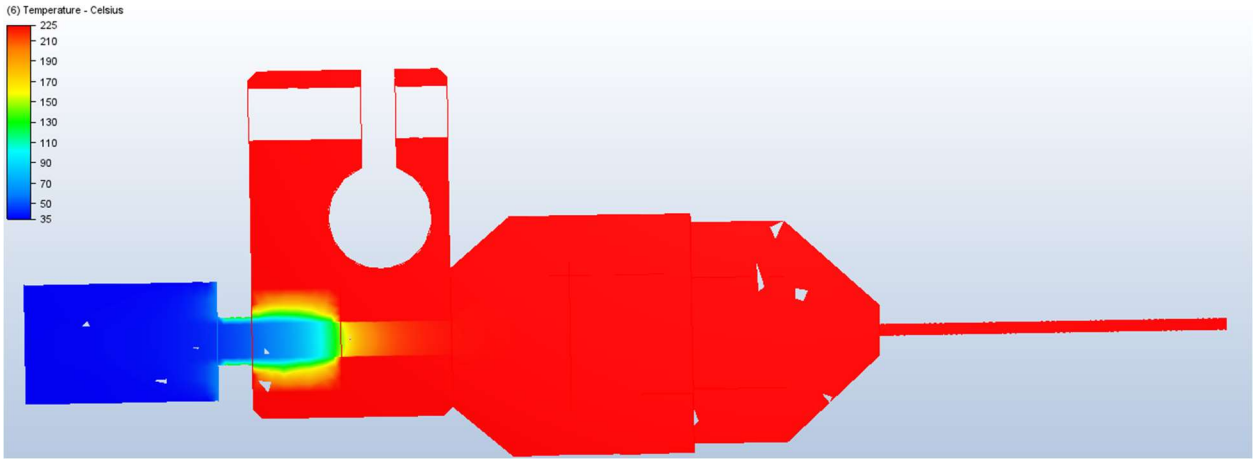

Figure 9: Thermal State of Prototype Extruder (T=299s)

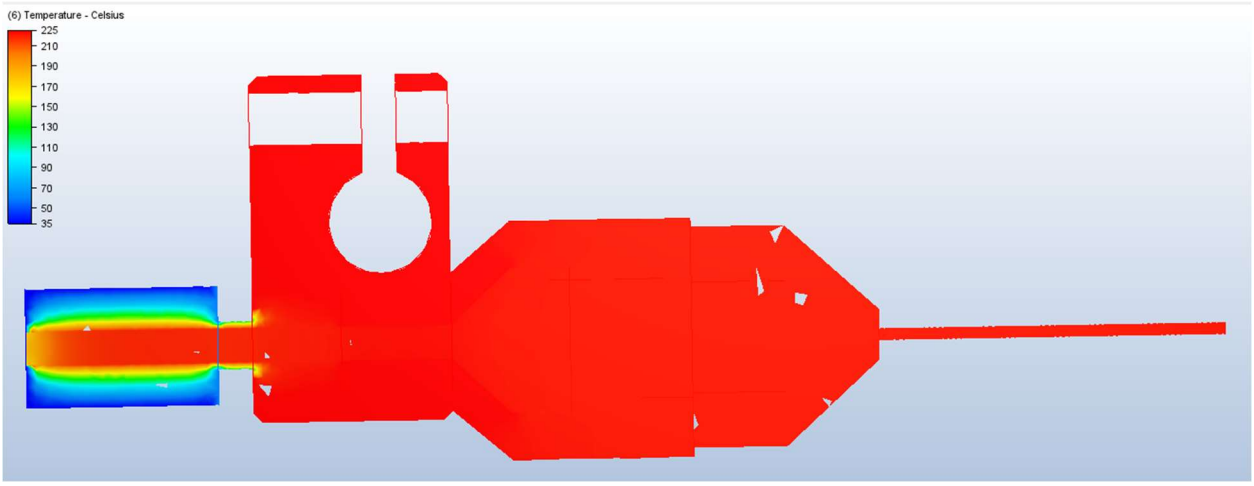

Figure 10: Thermal State of Prototype Extruder (T=316s)

It can be clearly seen in **Figures 9** and **10** that no matter how long the print is paused, due to the lack of cold filament being driven in to the hotend, the entire assembly will continue to heat up. In fact, if there was no heatsink or fan attached to the extruder, there would have been negative effects due to the filament melting to high in the hotend/heatsink. A graphical representation of this can be seen below in **Figure 11**. Specifically, this graph looks at the exit temperature of the nozzle to determine if the filament ever cools down to below 180ºC during the pause stage of the printing process. As you can see in the graph below, there is no point in which the filament will cool below to below 200ºC, let alone 180ºC. Important to note is that the end of the nozzle probe conducts pure filament and the nozzle, so the rapid ramp up in the first 100 seconds is due to no filament actually reaching the point, and the average temperature being calculated against the filament and wall of the nozzle.

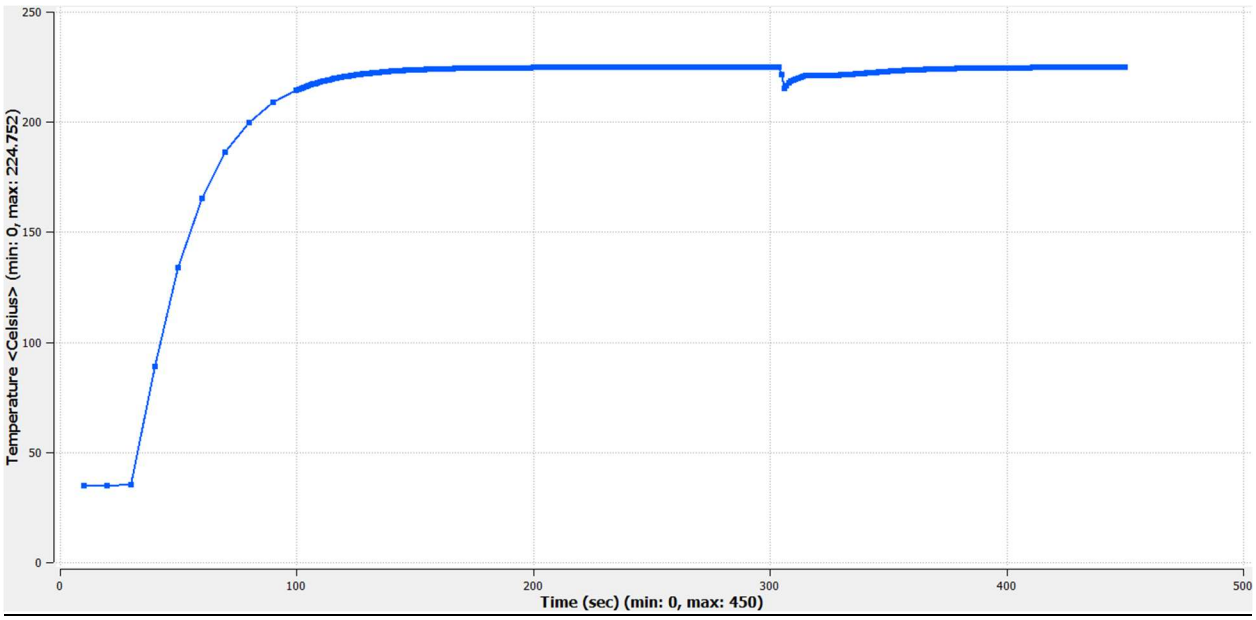

Figure 11: End of Nozzle Temperatures during Simulation

Conclusions and Future Work

The Z-pinning process for additive manufacturing has already shown in initial work to be an effective method for increasing Z-axis ultimate tensile strength as well as reducing anisotropy found in printed parts. However, defect propagation stymied the ability of longer and wider pins to effectively deposit good pins, reducing mechanical performance where increases were expected. As a result, a penetrating nozzle approach was proposed. The penetrating nozzle approach would combine the standard material deposition of stock FFF nozzles, while also introducing the ability to penetrate the pin cavity in order to lay a cleaner Z-pin deeper into the structure.

In order to quality a design before test prints could be conducted, two questions had to be answered before serious prototyping occurred. First, can material flow through the nozzle? Second, if material can flow, can it pause and then resume? The first question was answered by using a pressure drop analysis pioneered to quality how "printable" a system was. As a result of the rheological and geometric analysis of a mock-up of the penetrating nozzle, it was discovered that the critical pressure of the system was over 12Mpa. Which, when compared to the system pressure drop of 9.338Mpa, means that filament will flow through the system. This was verified through loading the material and performing a simple extrusion command in G-Code. To answer the second and final question, a full CFD analysis of the filament flow through the nozzle was conducted. As a result of this analysis, it was determined that once the extruder has been printing, the pause that occurs in standard Z-pinning is not long enough for significant cooling to occur. In fact, it was discovered that due to the nozzles proximity to the heating element, it will in fact continue to heat up until it reaches the system temperature of 225ºC. This was experimentally verified as well by pausing the printer after loading material and seeing filament continue to "ooze" out. Therefore, showing that even when the extruder had stopped depositing filament, the nozzle remained hot enough for residual filament to remain liquid inside the nozzle. After the pause, the extruder was able to resume deposition as well.

Due to these two pieces of analysis, it can be concluded that filament will flow through the penetrating nozzle design. For the future work in this method, microstructure analysis will be conducted to validate the effectiveness of the penetrating nozzle in regard to defect reduction as well as comparing the penetrating Z-pins, to standard Z-pins. Mechanical tensile testing will be conducted to determine if the penetrating nozzle was able to increase the tensile properties of the samples, either through defect elimination or improved interlocking.

Acknowledgements

Special thanks to Nathan Black and Alex Defilippis as well as the University of Tennessee Maker Space and Innovation and Collaboration study for their help in this project. Thanks to the U.S. Army Combat Capabilities Development Command Aviation & Missile Center as well for sponsoring this research. Additional support was generated under the National Science Foundation Award No. 2055529.

This research was sponsored by the Research sponsored by the U.S. Department of Energy, Office of Energy Efficiency and Renewable Energy, Advanced Manufacturing Office, under contract DE-AC05-00OR22725 with UT-Battelle, LLC.

References

[1] H. Bikas, P. Stavropoulos, G. Chryssolouris, Additive manufacturing methods and modelling approaches: a critical review, Int. J. Adv. Manuf. Technol. 83 (2016) 389–405. https://doi.org/10.1007/s00170-015-7576-2.

[2] S.S. Crump, Apparatus and method for creating three-dimensional objects, US5121329A, 1992. https://patents.google.com/patent/US5121329A/en (accessed June 28, 2022).

[3] A. Bellini, S. Güçeri, Mechanical characterization of parts fabricated using fused deposition modeling, Rapid Prototyp. J. 9 (2003) 252–264. https://doi.org/10.1108/13552540310489631.

[4] S. Ahn, M. Montero, D. Odell, S. Roundy, P.K. Wright, Anisotropic material properties of fused deposition modeling ABS, Rapid Prototyp. J. 8 (2002) 248–257. https://doi.org/10.1108/13552540210441166.

[5] O.S. Es-Said, J. Foyos, R. Noorani, M. Mendelson, R. Marloth, B.A. Pregger, Effect of Layer Orientation on Mechanical Properties of Rapid Prototyped Samples, Mater. Manuf. Process. 15 (2000) 107–122. https://doi.org/10.1080/10426910008912976.

[6] M.H. Too, K.F. Leong, C.K. Chua, Z.H. Du, S.F. Yang, C.M. Cheah, S.L. Ho, Investigation of 3D Non-Random Porous Structures by Fused Deposition Modelling, Int. J. Adv. Manuf. Technol. 19 (2002) 217–223. https://doi.org/10.1007/s001700200016.

[7] S. Shaffer, K. Yang, J. Vargas, M.A. Di Prima, W. Voit, On reducing anisotropy in 3D printed polymers via ionizing radiation, Polymer. 55 (2014) 5969–5979. https://doi.org/10.1016/j.polymer.2014.07.054.

[8] R.T.L. Ferreira, I.C. Amatte, T.A. Dutra, D. Bürger, Experimental characterization and micrography of 3D printed PLA and PLA reinforced with short carbon fibers, Compos. Part B Eng. 124 (2017) 88–100. https://doi.org/10.1016/j.compositesb.2017.05.013.

[9] A.R. Torrado Perez, D.A. Roberson, R.B. Wicker, Fracture Surface Analysis of 3D-Printed Tensile Specimens of Novel ABS-Based Materials, J. Fail. Anal. Prev. 14 (2014) 343–353. https://doi.org/10.1007/s11668-014-9803-9.

[10] A.R. Torrado, C.M. Shemelya, J.D. English, Y. Lin, R.B. Wicker, D.A. Roberson, Characterizing the effect of additives to ABS on the mechanical property anisotropy of specimens fabricated by material extrusion 3D printing, Addit. Manuf. 6 (2015) 16–29. https://doi.org/10.1016/j.addma.2015.02.001.

[11] C.E. Duty, V. Kunc, B. Compton, B. Post, D. Erdman, R. Smith, R. Lind, P. Lloyd, L. Love, Structure and mechanical behavior of Big Area Additive Manufacturing (BAAM) materials, Rapid Prototyp. J. 23 (2017) 181–189. https://doi.org/10.1108/RPJ-12-2015-0183.

[12] O. Eyercioglu, M. Aladag, S. Sever, Temperature evaluation and bonding quality of large scale additive manufacturing thin wall parts, Sigma J Eng Nat Sci. 36 (2018) 645–654.

[13] W. Zhong, F. Li, Z. Zhang, L. Song, Z. Li, Short fiber reinforced composites for fused deposition modeling, Mater. Sci. Eng. A. 301 (2001) 125–130. https://doi.org/10.1016/S0921-5093(00)01810-4.

[14] B.N. Turner, R.J. Strong, S.A. Gold, A review of melt extrusion additive manufacturing processes: I. Process design and modeling, Rapid Prototyp. J. (2014). https://doi.org/10.1108/RPJ-01-2013-0012.

[15] J.F. Rodríguez, J.P. Thomas, J.E. Renaud, Mechanical behavior of acrylonitrile butadiene styrene (ABS) fused deposition materials. Experimental investigation, Rapid Prototyp. J. 7 (2001) 148–158. https://doi.org/10.1108/13552540110395547.

[16] Q. Sun, G.M. Rizvi, C.T. Bellehumeur, P. Gu, Effect of processing conditions on the bonding quality of FDM polymer filaments, Rapid Prototyp. J. 14 (2008) 72–80. https://doi.org/10.1108/13552540810862028.
[17] J. Ghorbani, P. Koirala, Y.-L. Shen, M. Tehrani, Eliminating voids and reducing mechanical anisotropy in fused filament fabrication parts by adjusting the filament extrusion rate, J. Manuf. Process. 80 (2022) 651–658. https://doi.org/10.1016/j.jmapro.2022.06.026.
[18] V. Kishore, C. Ajinjeru, A. Nycz, B. Post, J. Lindahl, V. Kunc, C. Duty, Infrared preheating to improve interlayer strength of big area additive manufacturing (BAAM) components, Addit. Manuf. 14 (2017) 7–12. https://doi.org/10.1016/j.addma.2016.11.008.
[19] A. Kurapatti Ravi, A Study on an In-Process Laser Localized Pre-Deposition Heating Approach to Reducing FDM Part Anisotropy, M.S., Arizona State University, n.d. https://www.proquest.com/docview/1829549537/abstract/E227499866614B3APQ/1 (accessed September 1, 2021).
[20] C.E. Duty, J.A. (ORCID:0000000175271647) Failla, S. (ORCID:0000000250312585) Kim, J.M. (ORCID:0000000346350789) Lindahl, B.K. (ORCID:0000000214502250) Post, L.J. (ORCID:0000000259347135) Love, V. (ORCID:0000000344057917) Kunc, Reducing mechanical anisotropy in extrusion-based printed parts, Oak Ridge National Lab. (ORNL), Oak Ridge, TN (United States), 2017. https://www.osti.gov/biblio/1474689 (accessed September 2, 2021).
[21] C. Duty, J. Failla, S. Kim, T. Smith, J. Lindahl, V. Kunc, Z-Pinning approach for 3D printing mechanically isotropic materials, Addit. Manuf. 27 (2019) 175–184. https://doi.org/10.1016/j.addma.2019.03.007.
[22] S. Kim, T. Smith, J. Failla, J. Lindahl, V. Kunc, C. Duty, PARAMETRIC ANALYSIS ON VERTICAL PINS FOR STRENGTHENING EXTRUSION-BASED PRINTED PARTS, (n.d.) 11.
[23] Brenin Bales, Tyler Smith, Seokpum Kim, Vlastimil Kunc, Chad Duty, Geometric Parameter Analysis of Z-Pinning Additive Manufacturing, Addit. Manuf. (In Preperation).
[24] US Patent Application for PENETRATING AND ACTUATING NOZZLE FOR EXTRUSION-BASED 3D PRINTING Patent Application (Application #20190091927 issued March 28, 2019) - Justia Patents Search, (n.d.). https://patents.justia.com/patent/20190091927 (accessed January 13, 2022).
[25] S. Kim, T. Smith, J. Condon, A. Lambert, V. Kunc, C. Duty, GEOMETRIC PARAMETER ANALYSIS OF VERTICALLY EXTRUDED PINS FOR STRENGTH IMPROVEMENT IN ADDITIVE MANUFACTURING WITH FIBER-REINFORCED THERMOPLASTIC, (n.d.) 11.
[26] Brenin Bales, Tyler Smith, Seokpum Kim, Vlastimil Kunc, Chad Duty, DESIGN OF A PENETRATING DEPOSITION NOZZLE FOR Z-PINNING ADDITIVE MANUFACTURING, in: SAMPE 2022 Proc., SAMPE, Charlotte, North Carolina, 2022: pp. 880–894.
[27] C. Duty, C. Ajinjeru, V. Kishore, B. Compton, N. Hmeidat, X. Chen, A.A. Hassen, J. Lindahl, V. Kung, A Viscoelastic Model for Evaluating Extrusion-Based Print Conditions, in: 2017.
[28] Reusable Stainless Steel Dispensing Needle with 1/8 NPT Male Thread, 22 Gauge, McMaster-Carr. (n.d.). https://www.mcmaster.com/ (accessed July 11, 2022).
[29] Brass Pipe Adaptor 1/8" NPT Female - M6 Male Nickel Plated, REDUCER - Adaptors - Thread to Thread - Brass Fittings, (n.d.).

https://www.mettleair.com/store/brass/t2tmain/120main/brass-pipe-adaptor-1-8-npt-female-m6-male-nickel-plated-reducer.html (accessed July 11, 2022).
[30] C. Ajinjeru, Rheological evaluation and guidelines of high-performance amorphous thermoplastics and carbon fiber reinforced composites for additive manufacturing, (n.d.) 156.
[31] Prusament PLA Jet Black 1kg | Original Prusa 3D printers directly from Josef Prusa, Prusa3D Josef Prusa. (n.d.). https://www.prusa3d.com/product/prusament-pla-jet-black-1kg/#downloads (accessed July 11, 2022).
[32] C. Duty, A viscoelastic model for extrusion-based 3D printing of polymers what makes a material printable?, J Manuf Process Vol Submitt. No. 2017 (2017) 526–537.
[33] J.L. White, L. Czarnecki, H. Tanaka, Experimental Studies of the Influence of Particle and Fiber Reinforcement on the Rheological Properties of Polymer Melts, Undefined. (1980). https://www.semanticscholar.org/paper/The-influence-of-polymer-matrix-viscosity-on-the-of-Krivanek/dc40c434469b4e6b6a2856e4c4944606bacaef43 (accessed January 15, 2022).
[34] Brenin Bales, Nathan Black, Internal Temperature Verification, n.d.
[35] S. Yalçinkaya, M. Borak, B. Yildiz, M. Yildirim, THERMAL ANALYSIS OF A 3D PRINTER HOTEND AND NOZZLE, (2019) 8.